LIBRARY OF BIMETALLIC THREE WAYS CATALYSTS

Le Nguyen Vu

Directorate for Standards, Metrology and Quality – Quality Training Centre

Abstract: *Modern three-way catalysts in catalytic converters, used to control air pollution from automobiles, are still expensive and ineffective at light-off temperatures. Bimetallic nanoparticles were deemed to be the solution to this challenge. However, their superiority remains a myth due to the lack of uniformity in their synthetical methods performed by previous works. Therefore, to elucidate this ambiguity, an informative library of bimetallic three-way catalysts was constructed using a series of high-throughput experiments, which generate a massive quantity of data faster and more consistent than traditional experiments. The information from the library proved that bimetallic catalysts, with their intrinsic alloy synergism, are generally better than their mono-metallic counterparts and thereby suggested some ideas to engineer more powerful and economic alternatives substituting for the current conventional catalysts.*

Keywords: *Bimetallic nanoparticles, three-way catalysts, catalytic converter, alloys, high-throughput.*

Received 4 March 2023

Revised and accepted for publication 24 July 2023

Contact author: Le Nguyen Vu; Email: limaecho95@gmail.com

1. INTRODUCTION

One of the major sources of air pollution is surely automobiles. In modern transportation, three common harmful components found in vehicle exhaust gas are volatile organic compounds (VOC), carbon monoxide (CO), and nitrogen oxides (NO_x). In order to control the amount of these emission gases, catalytic converters, which contain three-way catalysts (TWC), have been equipped in vehicles. The three-way reactions convert harmful emissions into harmless ones, in which CO and VOC are oxidized into carbon dioxide (CO_2), while NO_x is reduced into nitrogen (N_2). The major component of a catalytic converter is a monolith substrate covered by a catalytic wash coat containing the three-way catalyst. Such wash coat generally contains catalytic active nanoparticles (NPs) of palladium (Pd), Platinum (Pt) and Rhodium (Rh), and high surface-area support materials such as -Al_2O_3 and CeO_2-ZrO_2. However, the hugest drawbacks of these elements are their high costs and their low abundance.[1,2] Furthermore, most commercial TWCs available can only convert emission gases effectively at temperatures above 300^{o}C,[3] thus the emission of a cold-start engine still contribute a significant portion to the total automobile's emission. In that regard, finding alternatives for the current catalytic particles is gaining great attention from both the industry and the academic.

Alloying two metal elements to obtain their synergistic effects is considered to be a strategy to achieve the target. This strategy allows the option of tuning a wide range of combinations with different elements and different ratios of contents. Several attempts to make bimetallic NPs have been made. For instance, K. Kusada et al. have successfully synthesized PdRu alloy NPs, which is more economical than Rh NPs.[4] Later, this bimetallic combination was proven to have superior catalytic activities to that of the mono counterparts and of Rh NPs in three-way reactions, by K. Sato .[5] Although many bimetallic systems have been reported,[3–5] their synthesizes were not conducted in a uniform manner causing the challenge in comparing the properties of those bimetallic systems and their mono-metallic counterparts in the most impartial and comprehensive way. As a consequence, the superiority of bimetallic catalysts over their monometallic relatives is remaining vague.[3,6]

Keep that in mind, in this research, a library of bimetallic particles, which are mainly combinations of Pd, Pt, and Rh with other metal elements, is prepared. One synthetic method with minor changes was employed and all synthesizes were done in homemade high-throughput (HTP) parallel synthetic reactors. The as–synthesized NPs later are loaded on support materials, such as -Al_2O_3, CeO_2-ZrO_2, and TiO_2, and evaluated using our in-house HTP screening instrument for TWC activities. The HTP experiment setups provide a reliable comparison and comprehensive information on bimetallic catalysts in a swifter manner than of separated traditional experiments. Thereby, the library suggests some potential economic alternatives for the current commercial catalysts.

2. EXPERIMENTAL SECTION

Material

Hydrogen tetrachloroaurate (III) trihydrate ($HAuCl_4$-$3H_2O$) was purchased from MP Biomedicals. Hydrogen hexachloroplatinate (IV) hexahydrate (H_2PtCl_6-$6H_2O$, ≥ 98.5%), potassium tetrachloropalladate (II) (K_2PdCl_4, 99%), rhodium (III) chloride trihydrate ($RhCl_3$-$3H_2O$, 99.5%), copper (II) chloride dihydrate ($CuCl_2$-$2H_2O$, 99%), triethylene glycol (99%), and polyvinylpyrrolodine ($(C_6H_9NO)_n$, K30, average MW = 40000) were purchased from Wako. Ruthenium (III) chloride hydrate ($RuCl_3$-xH_2O, Ru 46.8%) and iridium chloride hydrate ($IrCl_3$-xH_2O, Ir 54.6%) were purchased from Sigma Aldrich. Acetone, hexane, and methanol of research grade are purchased from Kanto Chemical. γ-Al_2O_3 (PURALOX SCFa100, SASOL, BET surface area of 106 m^2/g), TiO_2 (Aeroxide P25, EVONIK, BET surface area of 55 m^2/g), and CeO_2-ZrO_2 (nanosized, provided by Toyota Motor Corporation) were used as support materials.

Synthesis

All the samples were synthesized using an in-house parallel reactor setup, which has the maximum capacity of carrying 6 parallel reactions. In a particular reaction, 88 mg of polyvinylpyrrolidone (PVP) as a capping agent was dissolved in 20 ml of triethylene glycol (TEG) in a 40 ml glass vessel. In the cases of Cu-based bimetallic alloys, pH was controlled by adding an adequate amount of a 30% NaOH aqueous solution to adjust the pH of the TEG-PVP solution to 9. The solution was vigorously stirred under N_2, followed by heating to 190°C. Subsequently, 2.0 ml of an aqueous solution dissolving metal precursors (0.050 mmol per metal element) and 22 mg of PVP were swiftly injected into the TEG-PVP mixture. After a dark color

indicating the formation of NPs appeared, the reaction mixture was kept for 30 min, and then was naturally cooled to room temperature. Synthesized NPs were washed with an acetone/hexane mixture (3/1 v/v), and recovered by centrifugation, which was repeated three times. Finally, the product was re-dispersed and stored in methanol before use.

In catalyst preparation, 200 mg of support material and roughly 2 ml of a NPs solution were added into a 5 ml vial in order to have the final product containing 0.3 wt% of NPs. The suspension was then stirred thoroughly for 24 hours at 60°C with a parallel heating magnetic stirrer VELP AREX 6 equipped with MultilAluBlock. After that, the suspension was dried in an oven at 80°C overnight and then milled before being subjected to calcination for 2 hours at 550°C under a normal atmosphere. The calcined catalysts were milled to a fine powder and used for the catalytic test.

Characterization

Transmission electron microscopic (TEM) images were collected on a Hitachi H-7100 electron microscope operated at 100kV. A sample pool of 200 particles was taken to determine the average particle size and the particle size distribution. Powder X-ray diffraction (XRD) data were acquired on a Rigaku SmartLab X-ray diffractometer using a Cu-Kα radiation source. Elemental analysis was performed using a scanning electron microscope equipped with an energy-dispersive X-ray spectrometer (SEM-EDS, TM3030 Plus Microscope). EDS signals were captured at nine different locations on the dried sample droplet and averaged for deriving the chemical composition.

Catalyst evaluation

The HTP instrument consists of seven major components, a gas mixer, a flow distributor, a hollow furnace, quartz reaction tubes, an auto-sampler, a quadrupole mass-spectrometer (QMS, Transpector CPM 3, INFICON), and an exhausted system (**Figure 1)**.

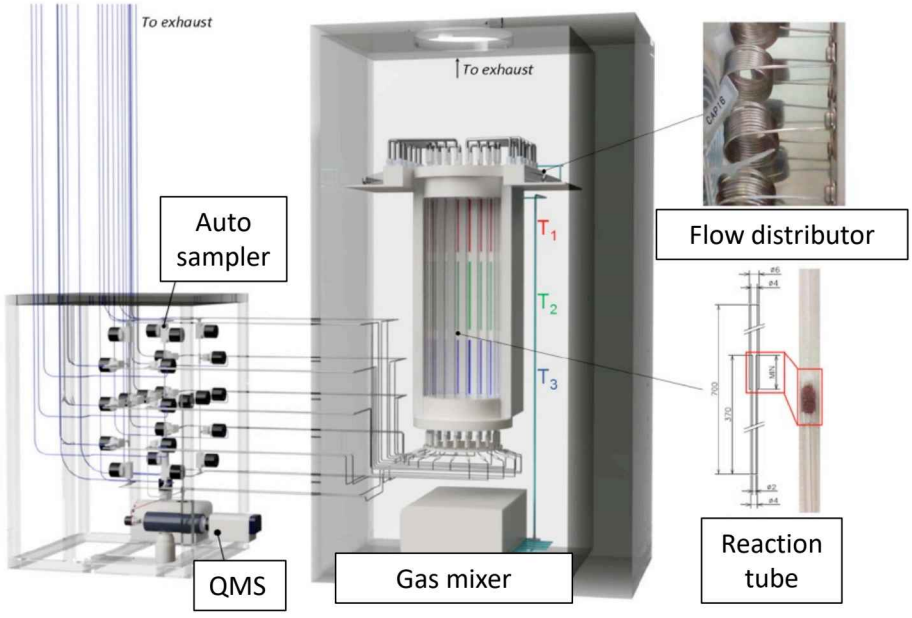

Figure 1: Schematic representation of a high-throughput screening system. Reproduced from Ref. [7].

First, the constituent gasses are mixed thoroughly in the gas mixer (MU-3504, HORIBA STEC) to make a model automobile exhaust gas with desired concentrations for each component (***Table 1***). Next, the mixed gas travels up to the flow distributor, where the flow is equally split into 20 channels. Later, the divided flows pass through 20 reaction quartz tubes located in the middle of the hollow furnace. Each quartz tube has inner diameters of 4 mm for the inlet end and 2 mm for the outlet end. Catalyst powder is fixed by quartz wool at the middle section of each tube, corresponding to the neck position between two different inner diameters. The furnace possesses three heating sectors and in each of which, a ceramic heater with a thermocouple is set. The heating program was set to rise from 100^{o}C to 400^{o}C with a ramping rate of 4^{o}C/min and for every 20^{o}C increment, the temperature is kept for half an hour in order to evaluate catalytic activity at that particular temperature before it continues to rise.

Table 1. Feed gas composition for three-way catalyst evaluation.

Feed gas component	Concentration (ppm)
CO	26000
C_3H_6	4000
NO	6000
O_2	28000
CO_2 (10%)	100000
He (83.6%)	836000

After the reaction, the effluent gas continues to enter the autosampler that is connected to the QMS. Auto sampling is performed by a programmed action sequence of pneumatically actuated diaphragm valves (MEGA ONE, Fujikin). In a typical sampling, a sampling time is 1.2 seconds followed by vacuum evacuation for 10 seconds. For one lap of measurement, the time is 224 seconds in total. Any leftover effluent gas is evacuated to the exhaust system. During the measurement, the sampled gas is continuously transferred from the autosampler to the QMS, and signals of pre-designated mass fractions are recorded. The light-off performance of catalysts was evaluated by the temperature of 50% conversion (T_{50}) for C_3H_6, CO, and NO, respectively.

Cluster analysis

Multiple correspondence analysis (MCA) was extracted from the variables by a scree test. The behavior of three-way catalysts is presented by different categorical variables including the presence/absence of constituent elements, support materials, and good/poor performances in the three reactions. When a T_{50} value for a certain conversion is below 300^{o}C, such a catalyst is attributed as good in terms of the mentioned conversions, and vice versa. The agglomerative hierarchical clustering (AHC) iteratively classifies catalysts based on the dissimilarity calculated from the reduced Euclidean distance of the three T_{50} values of the three reactions. Homogenous groups were created by the complete linkage method.

3. RESULT AND DISCUSSION

To keep synthesis conditions in constant, all metal precursors are salts or metal complexes of chloride. Furthermore, to understand the reducibility of each element, a molar ratio of 50/50

mol/mol was aimed in all syntheses. The characterization was conducted based on three analytical methods, SEM-EDS, TEM, and XRD. These methods were chosen due to their comprehension of characterization, availability, simplicity, and compatibility with the throughput of the other experiments.

SEM-EDS analysis

From ***Table 2***, the low uncertainty determined the homogeneity of EDS signals from nine measurement locations for all the bimetallic combinations, which later supports the XRD results indicating the successful formation of bimetallic alloys. Desired average element ratios of 50/50 were achieved in most of the cases, except RhCu even with pH control. Cu was the difficult element to be reduced completely due to its low reduction potential.

To achieve the desired elemental ratio for most of the Cu-based products, pH control (pH = 9) was required to gain more reduction power by generating more anionic species from TEG.[8] Despite the successful reduction, Cu NPs was unstable and oxidized after a few days when kept dispersed in methanol, thus the TEM image of this product is not available in the later section.

Table 2. Summary of successfully synthesized NPs and their characteristics

Name (AB)	Element A	Element B	Average element ratio (A : B, at%)	Crystal structure	Average particle size (nm)
Au	Au	-	-	Fcc	⩾100
Pt	Pt	-	-	Fcc	3.6 ± 0.6
Pd	Pd	-	-	Fcc	3.2 ± 0.9
Rh	Rh	-	-	Fcc	2.5 ± 0.4
Ru	Ru	-	-	Hcp	0.8 ± 0.1
Ir	Ir	-	-	Fcc	⩽ 0.7
AuRh	Au	Rh	46 : 54 ±0.5	Fcc	8.5 ± 2.5
AuPd	Au	Pd	46 : 54 ±0.6	Fcc	9.6 ± 1.7
AuPt	Au	Pt	50 : 50 ±0.5	Fcc	11.6 ± 2.1
PtRh	Pt	Rh	47 : 53 ±0.4	Fcc	2.8 ± 0.4
PdPt	Pd	Pt	55 : 45 ±1.0	Fcc	3.2 ± 0.4
PdRh	Pd	Rh	51 : 49 ±0.6	Fcc	2.7 ± 0.6
RhRu	Rh	Ru	51 : 49 ±1.5	Fcc	1.7 ± 0.3
PdRu	Pd	Ru	57 : 43 ±1.0	Fcc	2.6 ± 1.5
PtRu	Pt	Ru	47 : 53 ±1.0	Fcc	2.5 ± 0.6
RhIr	Rh	Ir	51 : 49 ±1.0	Fcc	1.7 ± 0.2
PdIr	Pd	Ir	57 : 43 ±0.4	Fcc	2.5 ± 0.5
PtIr	Pt	Ir	47 : 53 ±0.8	Fcc	2.1 ± 0.4
RhCu*	Rh	Cu	73 : 27 ±2.7	Fcc	1.7 ± 0.7
PdCu*	Pd	Cu	46 : 54 ±1.0	Fcc	2.6 ± 1.3
PtCu*	Pt	Cu	57 : 43 ±1.4	Fcc	2.0 ± 0.5
CuRh	Cu	Rh	6 : 94	Fcc	~ 1.2
*pH-controlled reduction with NaOH, in which pH = 9					

TEM analysis

Among all of the alloy species, AuRh, AuPd, and AuPt had average particle sizes of 8.5 ± 2.5 nm, 9.6 ± 1.7, and 11.6 ± 2.1 respectively, which were 3 to 10 times higher than those of the other bimetallic NPs in the library (***Table 2***). Furthermore, AuPt did not disperse well in methanol. Also, Au monometallic counterpart has the biggest sizes, in which the smallest particle has a diameter larger than 100 nm (***Figure 2***). These phenomena, which are later believed to be the major cause of Au's nano-species poor performance, are because of the low coordination of Au precursor with PVP. In fact, the synthesis of the other Au's nano-species, the addition of a small amount (22 mg) of PVP into the precursor solution was omitted for AuPt and Au to prevent clogging during hot-injection due to precipitation.

Nevertheless, bimetallic alloys of Cu, Ir, Pd, Pt, Rh, and Ru possess nicely uniform particle sizes distributions with small average size and excellent dispersion in methanol (***Figure 2 and Table 2***).

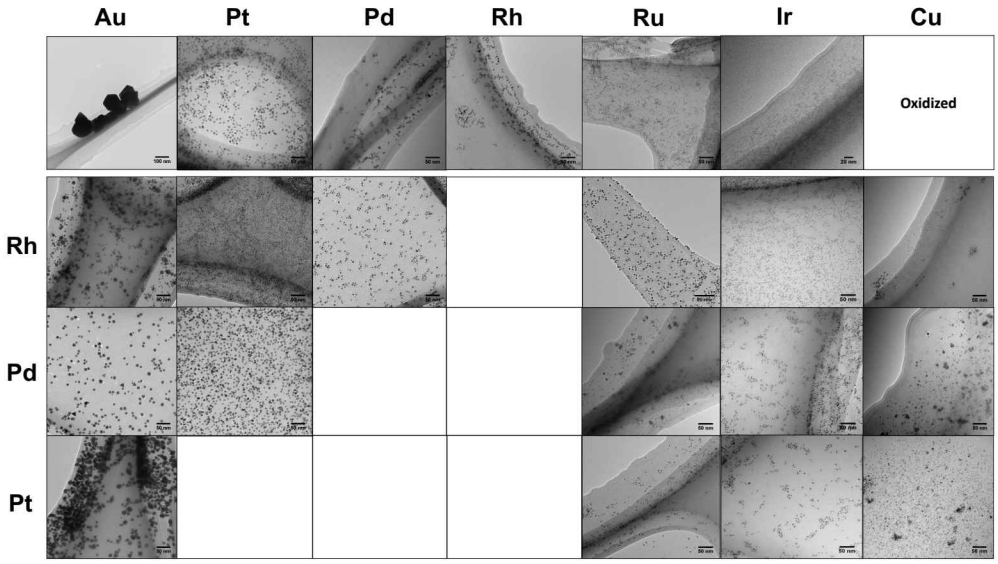

Figure 2: TEM image library of bimetallic NPs

XRD analysis

XRD analysis was employed in order to confirm the formation of bimetallic alloy by Vegard's law by identifying the peak position of the nano-alloy whether is located in between the peaks of the two monometallic counterparts. From the XRD patterns in ***Figure 3***, successful alloy formation was confirmed for all of the combinations among Au, Cu, Ir, Pd, Pt, Rh, and Ru. The face-centered cubic (fcc) is the dominant crystal structure in most of the cases except Ru monometallic, that exhibited the hexagonal close-packed (hcp) crystal lattice. In the cases of bimetallic alloys made of either Pt, Pd, or Ir, more careful consideration was required to assess their alloying since the references of those elements have very similar XRD peak positions and so do their alloys. The successful alloying was identified from the fact that the products were composed of a single crystalline phase and that the chemical composition was uniform in SEM-EDS. These would not be observed when a core-shell structure or a segregated structure was formed.

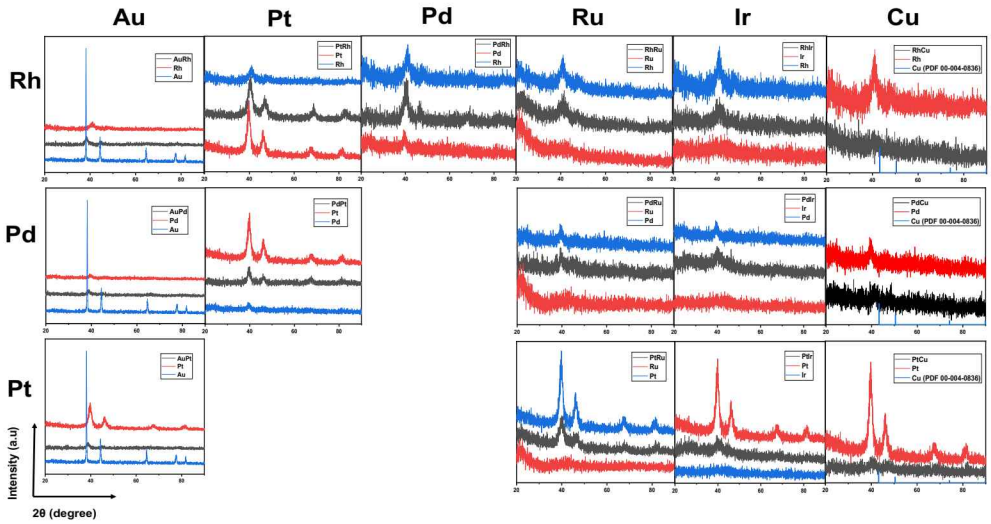

Figure 3: XRD library of bimetallic NPs

Catalyst evaluation

Total of 60 catalysts were prepared from 20 nano units of Au, Cu, Ir, Pd, Pt, Rh, and Ru, including 15 bimetallic combinations and 5 monometallic counterparts, by loading them on three different support materials of Al_2O_3, TiO_2, and CeO_2-ZrO_2. The missing T_{50}, in ***Figures 4-6*** demonstrated that AuPt on Al_2O_3 and CeO_2-ZrO_2 does not have any catalytic activities in the respective reactions. This could be due to the poor coordination mentioned above between Au's precursor and PVP.

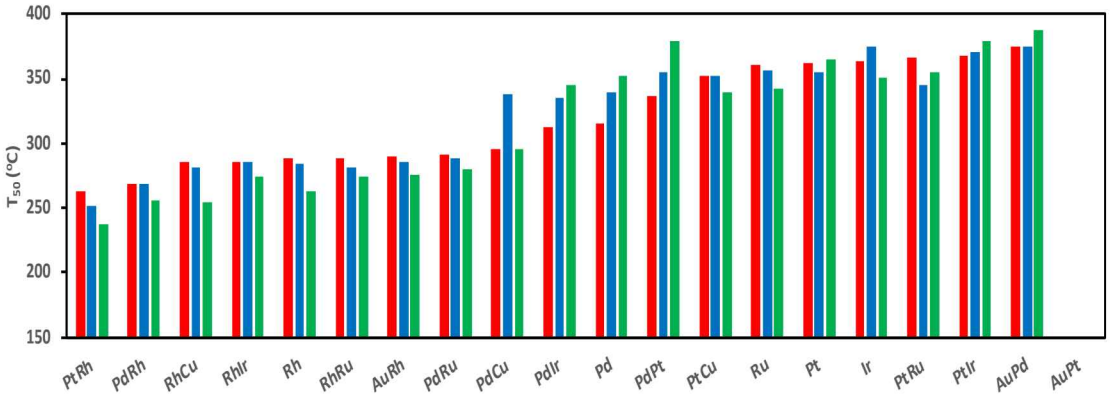

Figure 4: T_{50} comparison among C_3H_6 (red), NO (blue) and CO (green) conversion for Al_2O_3-based catalysts with performance ranking by C_3H_6 conversion.

In general, bimetallic catalysts with their unique alloy synergism, show better conversions than those of monometallic counterparts. Excellent combinations mostly contained Rh, which indicates that the three-way reactions favor Rh as an essential element. Bimetallic alloys such as AuRh, RhCu, RhRu, PdRh, and PtRh had very competitive performance to Rh monometallic NPs, hence it is obviously feasible to reduce the production cost of conventional TWC with lower cost elements than Rh while enhancing its activity by alloying with Rh. The general catalytic mechanism in supported noble metal NPs is the reversible redox process between the metal state, M^0, and an oxidized state MO_x.[6,9–12] The reason for Rh's superior activity in three-

way reactions perhaps is that each Rh atom can exchange 3 electrons while in other elements, such as Pd, Pt, and Cu, only 2 electrons are exchanged.[9,13]

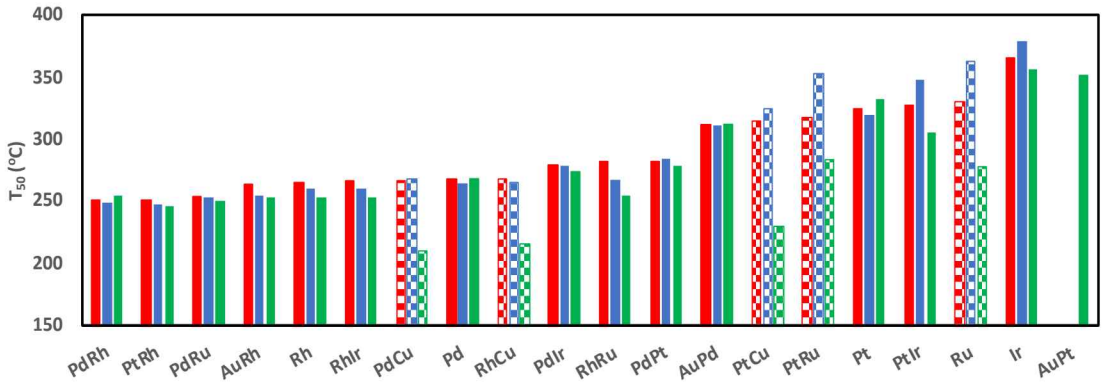

Figure 5: T_{50} comparison among C_3H_6 (red), NO (blue) and CO (green) conversion for CeO_2-ZrO_2 based catalysts with performance ranking by C_3H_6 conversion. Catalysts with selectivity toward CO oxidation are caro marked.

To emphasize the synergistic effect of alloy formation that makes bimetallic catalysts overall better than their mono-metallic counterparts, PtRh is looked deeper**.** As shown in ***Figures 4 and 5***, PtRh led to the best light-off performance in all three reactions. In addition, the majority of bimetallic alloys exhibited lower T_{50} values than their monometallic counterparts and this is absolutely in contrast with many previous statements.[3,6,9]

In the mid-1990s, a synergy between Pt and Rh was found.[14,15] Pt and Rh in their study were in form of separate monometallic NPs, rather than a bimetallic alloy. The proposed mechanism of the synergy described the stabilization of the Rh metal state by H_2 spillover from neighboring Pt particles. However, the feed gas in this study did not employ H_2 and only use CO as the main reductant. Thus, the outstanding performance of PtRh in this research is surely not alike to the same mechanism proposed by Hu. et al. but from alloy formation. The alloy synergism in PtRh could be understood by the Rh^{3+}-Rh^0 light-off redox process facilitated by Pt^{2+}. [9,16]

Furthermore, some non-rhodium-containing alloys like PdCu and PdRu also demonstrated the alloy synergistic, and proved themselves to be the more economical and more available alternatives for Rh. The result of PdRu from this library is likely consistent with that of PdRu synthesized by Kusada et al. and later by Sato et al. The reason behind PdRu's competitive catalytic activity to that of Rh is the formation of pseudo – Rh particles that mimic the electronic state of Rh NPs by alloying two immiscible elements, Pd and Ru.[4,5] Meanwhile, the remarkable catalytic activity of PdCu nano-alloy is likely explained due to the stabilization of the Pd metallic state, where is the adsorption site for hydrocarbon and CO, made by Cu when the alloy of Pd-Cu formed.[6,17–19].

The advantages of alloy formation do not only stop at the electronic complementary effect between two constituent elements but also extend to their intrinsic reciprocal metal-support interaction, which can be clearly seen in the evaluation results of CeO_2-ZrO_2-based catalysts. As seen in ***Figure 6***, the catalytical powers of NPs on CeO_2-ZrO_2 were overall better than their

equivalents on Al_2O_3 and TiO_2. The superiority of CeO_2-ZrO_2 in TWC conversion is due to the ability of CeO_2 to directly take part in the redox reactions where the reversible process between Ce^{3+} and Ce^{4+} occurs. Also, this redox process allows the material to store and release oxygen, thus it improves the catalytic power.[3,6,9,20]

Moreover, CeO_2 also owns extraordinary metal-support interaction[6,21–24-97] that appears to be the major explanation for the prevailing activity of the CeO_2 catalyst family. As evidence, Ru/CeO_2-ZrO_2 and PtRu/CeO_2-ZrO_2 exhibited much higher catalytic activity in CO conversion than their siblings of Al_2O_3 and TiO_2 (***Figure 6***). The phenomenon can be explained further by the CO removal mechanism of Ru involving the formation and stabilization of RuO_x as active species by CeO_2,[25,26] using the lattice oxygen migration mechanism.[21,22,27,28]

Once the labile oxygen from CeO_2-ZrO_2 covers the Ru constituent particles, more of RuO_x active site is generated on the catalyst surface, hence the CO conversion is enhanced. Extraordinary selectivity toward CO oxidation was also found in catalysts of Cu-containing alloys on CeO_2-ZrO_2 (***Figure 5***). Unlike C_3H_6 and NO conversions, where PtRh is still the champion of the rankings, PdCu, RhCu, and PtCu are the top three catalysts in the CO conversion (***Figure 6***). This tremendous selectivity towards CO oxidation can be clearly seen in PtCu/CeO_2-ZrO_2, which performed poorly in NO and C_3H_6 conversions (***Figure 5***).

Before this work, Abdelsayed et al. reported relevant results,[29] where PdCu, RhCu, and PtCu loaded on CeO_2 exhibited better CO conversion than PtRh and PdRh. The promotion effect could be from the formation of Cu^+ species that play a role as highly selective chemisorption sites for CO when Cu's nano-species are loaded on CeO_2-based materials.[17,18,30]

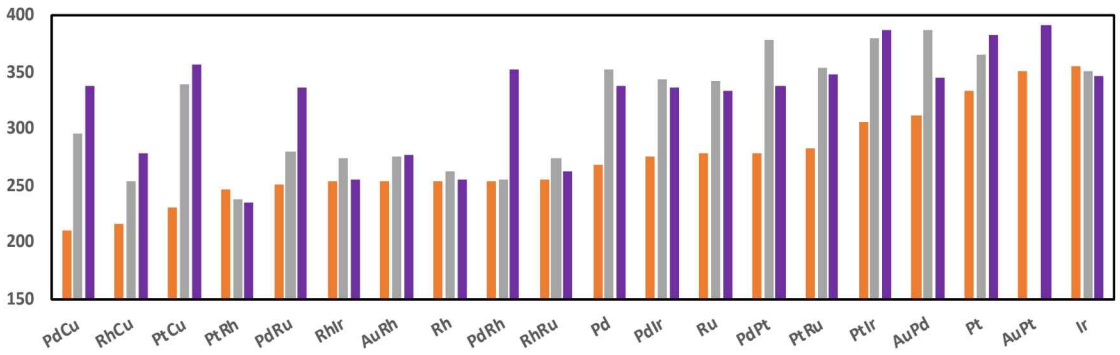

Figure 6: Catalytic activity comparison of bimetallic and monometallic NPs loaded on different supports in CO oxidation by T_{50}: CeO_2-ZrO_2 (orange), Al_2O_3 (gray) and TiO_2 (purple).

Special interaction between CeO_2 and metal NPs is significantly emphasized in the cases of Pd's products loading on CeO_2-ZrO_2, especially of PdRu and PdCu, which became tremendously competitive with the Rh counterparts in all three reactions (***Figure 5***).

The enhancement of the catalytic activity of Pd when on CeO_2 or relevant materials can be generally explained by the ability of CeO_2 to stabilize the intermediate Pd(I) oxidation state which greatly boosts the elimination of C_3H_6 and CO.[6,31].

The results from the catalyst evaluation unveil that the catalytic performance is majorly influenced by the choice of metal elements and support material, which later can be clearly seen in the cluster analysis.

Cluster analysis

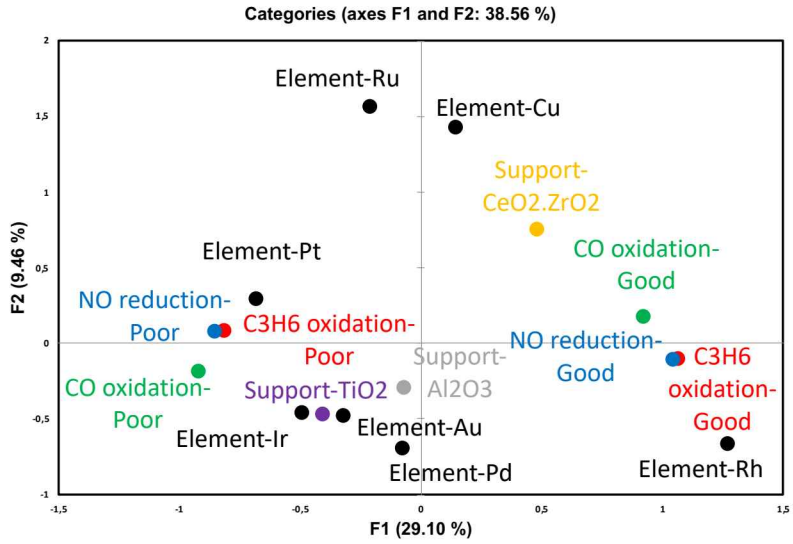

Figure 7: Symmetric plot in multiple correspondence analysis for 60 catalysts

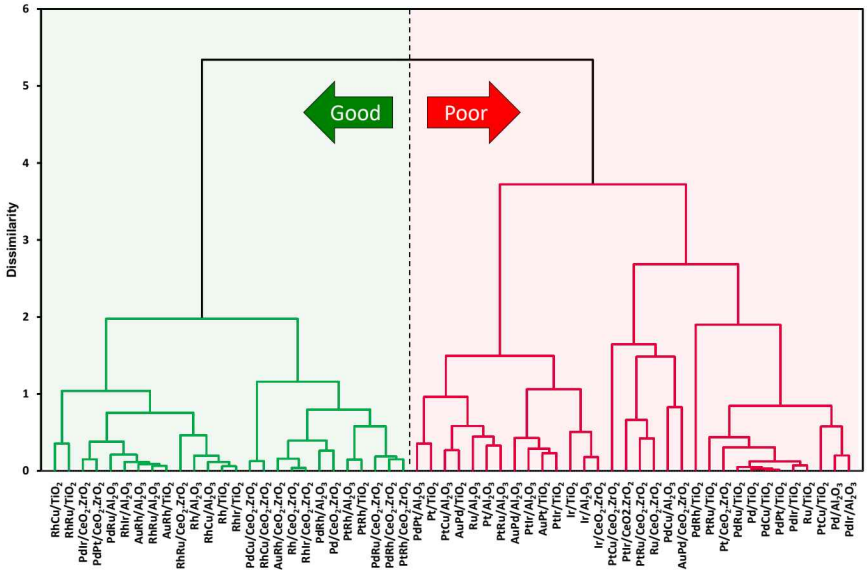

Figure 8: Dendrogram of agglomerative hierarchical clustering of 58 catalysts. AuPt/Al_2O_3 and AuPt/CeO_2-ZrO_2 were omitted due to the lack of (a part of) T_{50} values

Collinearity among the three reactions can be easily seen in the symmetric plot made by MCA (***Figure 7***) at the closeness between good performances dots in the three reactions as well as between the poor performance ones, indicating that catalysts with good catalytic activities in one reaction tend to have good activities in other two and vice versa. The catalytic activities mostly depend on the choice of metal elements and support material. The predominance in performance of Rh-containing catalysts and CeO_2-ZrO_2 based catalysts are described by the proximity of the representing dots to those of good reactions. On the other hand, the unfavorable parameters such as Pt, Ir, Au, and TiO_2 are presented by the cluster with the poor performance dots. This trending relatively agreed with the one in the dendogram (***Figure 8***) made by AHC. Other variables, "support-Al_2O_3", "element-Pd", "element-Cu", and "element-Ru" scatter

between good performance dots and poor performance dots, indicating that depending on the combination, catalysts that possess these constituents can either have good or poor catalytic performances. Indeed, as described above, alloys of Pd, Cu, and Ru exhibited higher performances when loaded on CeO_2-ZrO_2 than those loaded on Al_2O_3 or TiO_2.

4. CONCLUSION

In this work, a unified synthetic method and high-throughput reactor setups were employed to conduct a series of high-throughput experiments and analysis. Thereby, an informative library of 45 bimetallic TWC catalysts accompanied with 15 of their mono-metallic siblings was successfully constructed. The reduction potential gap between two constituents is the major challenge in the synthesis of bimetallic NPs. It was proven that bimetallic alloys have superior catalytic activities in three-way reactions compared to their monometallic counterparts. The improvement in the catalytic power of bimetallic alloys certainly comes from the synergistic effect of alloying metallic elements. Moreover, the library highlighted the important relationship between the choices of elements and support materials. Thereby, it widely ramifies a diversity of possible strategies to improve three-way catalyst performance as well as to lower its manufacturing costs, such as alloying Rh with less costly elements or using non-rhodium combinations like PdCu/CeO_2-ZrO_2 and PdRu/CeO_2-ZrO_2.

**** Acknowledgment:*** *This work was supported by Japan Advanced Institute of Science and Technology (JAIST) and Toyota Motor Corporation. All experiments and analysis were conducted at JAIST. Support materials were provided by Toyota Motor Corporation. Sincere gratitude to Taniike laboratory's members for assisting in completion of this work.*

REFERENCE

1. Ore, I. *et al.* (2021). *Mineral Commodity Summaries.*
2. Hans Wedepohl, K. (1995). The composition of the continental crust. *Geochim. Cosmochim. Acta* Issue **59**, pp. 1217–1232.
3. Rood, S., Eslava, S., Manigrasso, A. & Bannister, C. (2020). Recent advances in gasoline three-way catalyst formulation: A review. *Proc. Inst. Mech. Eng. Part D J. Automob. Eng.* **234**, pp. 936–949.
4. Kusada, K. *et al.* (2014). Solid solution alloy nanoparticles of immiscible Pd and Ru elements neighboring on Rh: Changeover of the thermodynamic behavior for hydrogen storage and enhanced co-oxidizing ability. *J. Am. Chem. Soc.* Issue **136**, pp. 1864–1871.
5. Sato, K. *et al.* (2016). A Synthetic Pseudo-Rh: NO_x Reduction Activity and Electronic Structure of Pd–Ru Solid-solution Alloy Nanoparticles. *Sci. Rep.* Issue **6**, 28265.
6. Wang, J., Chen, H., Hu, Z., Yao, M. & Li, Y. (2015). A review on the Pd-based three-way catalyst. *Catal. Rev. - Sci. Eng.* Issue **57**, pp. 79–144.
7. Nguyen, T. N. *et al.* (2020). High-Throughput Experimentation and Catalyst Informatics for Oxidative Coupling of Methane. *ACS Catal.* Issue **10**, pp. 921–932.
8. Fievet, F. *et al.* (2018). The polyol process: a unique method for easy access to metal nanoparticles with tailored sizes, shapes and compositions. *Chem. Soc. Rev.* Issue **47**, pp. 5187–5233.
9. Li P, Chen X, Li Y, Schwank JW. (2019). A review on oxygen storage capacity of CeO_2-based materials: Influence factors, measurement techniques, and applications in reactions related to catalytic automotive emissions control. *Catal Today*. Issue **327**, pp. 90-115

10. Asakura, H. *et al.* (2018). Dynamic Behavior of Rh Species in Rh/Al_2O_3 Model Catalyst during Three-Way Catalytic Reaction: An Operando X-ray Absorption Spectroscopy Study. *J. Am. Chem. Soc.* Issue **140**, pp. 176–184.

11. Hosokawa, S. *et al.* (2005). Oxidation characteristics of Ru/CeO_2 catalyst. *Appl. Catal. A Gen.* Issue **288**, pp. 67–73.

12. Dey, S. & Dhal, G. C. (2020). Applications of Rhodium and Ruthenium Catalysts for CO Oxidation: an Overview. *Polytechnica* Issue **3**, pp. 26–42.

13. Gayen, A. *et al.* $Ce_{1-x}Rh_xO_{2-\delta}$ solid solution formation in combustion-synthesized Rh/CeO_2 catalyst studied by XRD, TEM, XPS, and EXAFS. *Chem. Mater.* **16**, 2317–2328 (2004).

14. Hu, Z. *et al.* (1998). Performance and structure of Pt-Rh three-way catalysts: Mechanism for Pt/Rh synergism. *J. Catal.* Issue **174**, pp. 13–21.

15. Z.Hu, (1996). A Pt-Rh synergism in Pt/Rh three-way catalysts. Chem. Commun., pp 879–880.

16. Gayen, A., Baidya, T., Biswas, K., Roy, S. & Hegde, M. S. (2006). Synthesis, structure and three way catalytic activity of $Ce_{1-x}Pt_x/2Rh_x/2O_{2-\delta}$ (x = 0.01 and 0.02) nano-crystallites: Synergistic effect in bimetal ionic catalysts. *Appl. Catal. A Gen.* Issue **315**, pp. 135–146.

17. Hungría, A. B. *et al.* (2002). Effects of copper on the catalytic properties of bimetallic Pd-Cu/(Ce, Zr)O_x/Al_2O_3 and Pd-Cu/(Ce, Zr)O_x catalysts for CO and NO elimination. *J. Catal.* Issue **206**, pp. 281–294.

18. Fernández-García, M. *et al.* (2000). Behavior of palladium-copper catalysts for CO and NO elimination. *J. Catal.* Issue **190**, pp. 387–395.

19. Shinjoh, H. (2006). Rare earth metals for automotive exhaust catalysts. *J. Alloys Compd.* Issue **408–412**, pp. 1061–1064.

20. Li, P., Chen, X., Li, Y. & Schwank, J. W. (2019). A review on oxygen storage capacity of CeO_2 - based materials: Influence factors, measurement techniques, and applications in reactions related to catalytic automotive emissions control. *Catal. Today* Issue **327**, pp. 90–115.

XÂY DỰNG THƯ VIỆN VỀ XÚC TÁC KHÍ THẢI Ô TÔ HỢP KIM HAI NGUYÊN TỐ

Tóm tắt: *Xúc tác khí thải thương mại hiện nay vẫn có giá thành sản xuất cao và không hoạt động hiệu quả tại thời điểm động cơ lạnh mới mới khởi động. Việc sử dụng hạt nano của hợp kim hai nguyên tố được cho là giải pháp của vấn đề này. Tuy nhiên, sự ưu việt của hạt nano hợp kim so với hạt đơn nguyên tố chưa được chứng minh rõ ràng, do các nghiên cứu trước không có sự đồng nhất trong phương pháp điều chế. Do đó, trong bài báo này, thư viện thông tin về hạt nano hợp kim hai nguyên tố được xây dựng bằng một chuỗi các thí nghiệm thông lượng cao trên cơ sở phương pháp tổng hợp thống nhất với thiết lập lò phản ứng thông lượng cao cho phép cho ra nhiều kết quả nhanh hơn và nhất quán hơn so với các thí nghiệm truyền thống. Các thông tin từ thư viện này đã chứng minh rằng hiệu quả xúc tác của xúc tác hợp kim hai nguyên tố là ưu việt hơn so với xúc tác đơn nguyên tố tương ứng và từ đó đưa ra các ý tưởng thiết kế các loại xúc tác mới có hoạt tính cao hơn và rẻ hơn thay thế cho các loại xúc tác truyền thống.*

Từ khóa: *Hạt nano lưỡng kim, chất xúc tác ba chiều, bộ chuyển đổi xúc tác, hợp kim, thông lượng cao.*